

Vortex state in double transition superconductors

Yasushi Matsunaga,* Masanori Ichioka,† and Kazushige Machida‡

Department of Physics, Okayama University, Okayama 700-8530, Japan

(Dated: September 26, 2018)

Novel vortex phase and nature of double transition field are investigated by two-component Ginzburg-Landau theory in a situation where fourfold-twofold symmetric superconducting double transition occurs. The deformation from 60° triangular vortex lattice and a possibility of the vortex sheet structure are discussed. In the presence of the gradient coupling, the transition changes to a crossover at finite field. These characters are important to identify the multiple superconducting phase in $\text{PrOs}_4\text{Sb}_{12}$.

PACS numbers: 74.25.Qt, 74.20.Rp, 74.20.De, 74.25.Dw

In the newly discovered superconductor $\text{PrOs}_4\text{Sb}_{12}$, which is a heavy-fermion compound with filled skutterudite structure, a novel pairing mechanism is considered in connection to quadrupole fluctuations [1]. Several experimental results suggest unconventional pairing symmetry. In the nuclear spin-lattice relaxation experiment, the coherence peak is absent below the transition temperature T_c , and the low temperature behavior indicates that $\text{PrOs}_4\text{Sb}_{12}$ has full gap or point nodes, excluding line nodes, at a zero field [2]. The specific heat jump at T_c shows double transition [3]. The thermal transport measurement in the magnetic field rotated in the ab -plane of the crystal axes reveals the phase diagram of the double transition, and shows that a fourfold-symmetric pairing function around the c -axis in the high-field H-phase is changed to a twofold-symmetric one in the low-field L-phase at the second transition field H^* , when magnetic field or temperature is decreased [4]. Thus, the H - T phase diagram is divided into two regions, H- and L-phases. The muon spin relaxation (μSR) experiment reports the spontaneous moment in the superconducting phase [5]. These results indicate an unconventional pairing of the superconductivity in $\text{PrOs}_4\text{Sb}_{12}$.

To explain the double transition, we need multiple components for the pairing functions. The fourfold-twofold transition in $\text{PrOs}_4\text{Sb}_{12}$ can be explained as follows: After the fourfold-symmetric pairing component appears at the first transition, the second component appears at the second transition, and the combination of these components gives rise to the twofold-symmetric gap structure. For $\text{PrOs}_4\text{Sb}_{12}$, the scenario of “anisotropic- s ”+ id -wave pairing with point nodes was proposed, and the double transition is analyzed by the Ginzburg-Landau (GL) theory at a zero field [6]. In the vortex states at finite fields, however, this fourfold-twofold transition is not a true transition, when the gradient coupling terms are present in the GL theory [7]. That is, the twofold component at the L-phase is induced by the gradient coupling, and produces twofold symmetric behavior in addition to fourfold symmetric one, even in the H-phase above H^* . To avoid the mixing of the twofold component above H^* , the plausible

pairing symmetry should be a triplet pairing where d -vector of the two components are orthogonal each other (i.e., $\mathbf{d}_1^* \cdot \mathbf{d}_2 = 0$), so that the gradient coupling terms vanish [7].

On the other hand, in multi-component superconductors, it is interesting to examine the possibility of exotic vortex states, such as a coreless vortex [8, 9, 10, 11, 12, 13, 14]. In this letter, we investigate the double transition by the two-component GL theory in the magnetic field, and calculate the vortex structure by the time-evolution of the time-dependent GL (TDGL) equation.

First, we derive two-component GL equation appropriate to study the fourfold-twofold transition in $\text{PrOs}_4\text{Sb}_{12}$. The pair potential in 2×2 matrix form is decomposed to two components as $\hat{\Delta}(\mathbf{r}, \mathbf{k}) = \eta_1(\mathbf{r})\hat{\phi}_1(\mathbf{k}) + \eta_2(\mathbf{r})\hat{\phi}_2(\mathbf{k})$ with the order parameter $\eta_m(\mathbf{r})$, where \mathbf{r} is the center of mass coordinate of the Cooper pair and $m = 1, 2$. The relative momentum \mathbf{k} of the pair is mapped on the Fermi surface. The pairing function is given by $\hat{\phi}_m(\mathbf{k}) = i\hat{\sigma}_y\phi_m(\mathbf{k})$ for the singlet pairing, and $\hat{\phi}_m(\mathbf{k}) = i\sum_{j=x,y,z} d_{m,j}(\mathbf{k})\hat{\sigma}_j\hat{\sigma}_y$ for the triplet pairing with Pauli matrices $\hat{\sigma}_x, \hat{\sigma}_y, \hat{\sigma}_z$. We assume that the superconducting gap by $\hat{\phi}_1(\mathbf{k})$ ($\hat{\phi}_2(\mathbf{k})$) has fourfold (twofold) symmetry [6, 7], and that the transition temperature estimated from the pairing interaction is lower for the second component, i.e., $T_c = T_{c1} > T_{c2}$. Since the pairing symmetry for $\text{PrOs}_4\text{Sb}_{12}$ is not established yet, the pairing function forms $\hat{\phi}_m(\mathbf{k})$ are not specified in this study.

Within the GL approximation, the free energy in the superconducting state is generally given by $F_s = F_n + \int f(\mathbf{r})d\mathbf{r}$ with

$$f(\mathbf{r}) = -\alpha_0(T_c - T)|\eta_1|^2 - \alpha_0(T_{c2} - T)|\eta_2|^2 + |A_2| \left\{ \left\langle \frac{1}{2} \text{tr}(\hat{\Delta}^\dagger(\mathbf{v} \cdot \mathbf{q})^2 \hat{\Delta}) \right\rangle + \left\langle \frac{1}{2} \text{tr}(\hat{\Delta}^\dagger \hat{\Delta} \hat{\Delta}^\dagger \hat{\Delta}) \right\rangle \right\} \quad (1)$$

in the clean limit [15], where $\mathbf{q} = (\hbar/i)\nabla + (2\pi/\phi_0)\mathbf{A}$, F_n is the free energy in the normal state, $|A_2| = 7\zeta(3)/(16\pi^2 T_c^2)$ with Riemann's ζ -function, ϕ_0 is a flux quantum, \mathbf{v} is a Fermi velocity, $\langle \cdots \rangle$ indicates the Fermi surface average of \mathbf{k} , and \mathbf{A} is a vector potential. Since the magnetic field is applied along the z -axis, $q_z = 0$.

In the dimensionless form, Eq. (1) is written as

$$\begin{aligned} \tilde{f} \equiv \frac{f}{f_0} = & - \left(1 - \frac{T}{T_c}\right) |\eta_1|^2 - \left(\frac{T_{c2}}{T_c} - \frac{T}{T_c}\right) |\eta_2|^2 \\ & + \eta_1^*(q_x^2 + q_y^2)\eta_1 + C_{22x}\eta_2^*q_x^2\eta_2 + C_{22y}\eta_2^*q_y^2\eta_2 \\ & + C_{12x}\eta_1^*q_x^2\eta_2 + C_{12x}\eta_2^*q_x^2\eta_1 \\ & + C_{12y}\eta_1^*q_y^2\eta_2 + C_{12y}\eta_2^*q_y^2\eta_1 \\ & + \frac{1}{2}\{|\eta_1|^4 + C_2|\eta_2|^4 + 4C_3|\eta_1|^2|\eta_2|^2 \\ & + C_4^*\eta_1^{*2}\eta_2^2 + C_4\eta_2^{*2}\eta_1^2\}, \end{aligned} \quad (2)$$

using $f_0 = \alpha_0 T_c \eta_0^2$, $\eta_0^2 = \alpha_0 T_c / (2|A_2|C_1) \equiv 1$ and $\xi_0^2 = |A_2|C_{11x}/(\alpha_0 T_c) \equiv 1$. The coefficients of the gradient terms in Eq. (2) are given by

$$\begin{aligned} C_{11x} &= \langle |\phi_1|^2 v_x^2 \rangle = \langle |\phi_1|^2 v_y^2 \rangle, \\ C_{22x} &= \langle |\phi_2|^2 v_x^2 \rangle / C_{11x} \equiv (1 - c) / (X \sqrt{1 - c^2}), \\ C_{22y} &= \langle |\phi_2|^2 v_y^2 \rangle / C_{11x} \equiv (1 + c) / (X \sqrt{1 - c^2}), \\ C_{12x} &= \langle \phi_1^* \phi_2 v_x^2 \rangle / C_{11x}, \quad C_{12y} = \langle \phi_1^* \phi_2 v_y^2 \rangle / C_{11x}, \end{aligned} \quad (3)$$

where $\overline{\phi_m^* \phi_n} \equiv \phi_m^* \phi_n$ for the singlet pairing, $\overline{\phi_m^* \phi_n} \equiv \mathbf{d}_m^* \cdot \mathbf{d}_n$ for the triplet pairing and $|\phi_m|^2 \equiv \overline{\phi_m^* \phi_m}$. The slope ratio of H^* and H_{c2} in the H - T phase diagram is roughly given by $X = [\langle |\phi_1|^2 v_x^2 \rangle \langle |\phi_1|^2 v_y^2 \rangle / \langle |\phi_2|^2 v_x^2 \rangle \langle |\phi_2|^2 v_y^2 \rangle]^{1/2}$. To reproduce the experimentally obtained H^* behavior, it is appropriate to use $X \sim H^*/H_{c2} \sim 0.5$. In Eq. (3), c is an anisotropic parameter related to the second order parameter. When $|\phi_2|^2$ has two-fold symmetry under the rotation around the z -axis, c is not zero since $\langle |\phi_2|^2 v_x^2 \rangle \neq \langle |\phi_2|^2 v_y^2 \rangle$. C_{12x} and C_{12y} reflect the strength of the gradient coupling between η_1 and η_2 .

The coefficients of the quadratic terms in Eq. (2) are given by $C_1 = \langle |\phi_1|^4 \rangle$, $C_2 = \langle |\phi_2|^4 \rangle / C_1$, $C_3 = \langle |\phi_1|^2 |\phi_2|^2 \rangle / C_1$, $C_4 = \langle \phi_1^{*2} \phi_2^2 \rangle / C_1$ for the singlet pairing, and $C_1 = \langle 2|\mathbf{d}_1|^4 - |\mathbf{d}_1 \cdot \mathbf{d}_1|^2 \rangle / C_1$, $C_2 = \langle 2|\mathbf{d}_2|^4 - |\mathbf{d}_2 \cdot \mathbf{d}_2|^2 \rangle / C_1$, $C_3 = \langle |\mathbf{d}_1|^2 |\mathbf{d}_2|^2 + |\mathbf{d}_1^* \cdot \mathbf{d}_2|^2 - |\mathbf{d}_1 \cdot \mathbf{d}_2|^2 \rangle / C_1$, $C_4 = \langle 2(\mathbf{d}_2^* \cdot \mathbf{d}_1)^2 - (\mathbf{d}_2^* \cdot \mathbf{d}_2^*)(\mathbf{d}_1 \cdot \mathbf{d}_1) \rangle / C_1$ for the triplet pairing. However, we can not identify the definitive values of coefficients in Eq. (2) for $\text{PrOs}_4\text{Sb}_{12}$, because the detailed information of the pairing function and Fermi surface structure have not been established yet. It is noted that the Fermi surface anisotropy also largely affects on the coefficients. Therefore, we treat these coefficients as arbitrary parameters, and report some typical results obtained in this framework.

Before considering vortex states, we study a uniform state at a zero field. From the free energy minimum condition, the relative phase of η_1 and η_2 becomes $(\alpha \pm \pi)/2$ with α given by $C_4 = |C_4|e^{i\alpha}$. For the H-phase, $\eta_1 = (1 - T/T_c)^{1/2}$ and $\eta_2 = 0$. The second component η_2 appears at the lower transition temperature T^* given by

$$\frac{T^*}{T_c} = \frac{T_{c2}/T_c - (2C_3 - |C_4|)}{1 - (2C_3 - |C_4|)}, \quad (4)$$

which is derived by linearizing the equation $\partial \tilde{f} / \partial \eta_2^* = 0$. In the presence of η_1 , T^* is suppressed compared with T_{c2} . To assure that $T^* > 0$, we have to satisfy $2C_3 - |C_4| < T_{c2}/T_c$.

The vortex structure is calculated by the time-evolution following the TDGL equation coupled with Maxwell equation [16, 17],

$$\frac{\partial}{\partial t} \eta_1 = -\frac{1}{12} \frac{\partial \tilde{f}}{\partial \eta_1^*}, \quad \frac{\partial}{\partial t} \eta_2 = -\frac{1}{12} \frac{\partial \tilde{f}}{\partial \eta_2^*}, \quad (5)$$

$$\frac{\partial}{\partial t} \mathbf{A} = \tilde{\mathbf{j}}_s - \kappa^2 \nabla \times \mathbf{B}, \quad \mathbf{B} = \nabla \times \mathbf{A}. \quad (6)$$

The supercurrent $\tilde{\mathbf{j}}_s = (\tilde{j}_{s,x}, \tilde{j}_{s,y}) \propto (\partial \tilde{f} / \partial A_x, \partial \tilde{f} / \partial A_y)$ is given by

$$\begin{aligned} \tilde{j}_{s,x} &= \text{Re}[\eta_1^*(q_x \eta_1) + C_{22x}\eta_2^*(q_x \eta_2) \\ &+ C_{12x}\eta_1^*(q_x \eta_2) + C_{12x}^*\eta_2^*(q_x \eta_1)], \end{aligned} \quad (7)$$

$$\begin{aligned} \tilde{j}_{s,y} &= \text{Re}[\eta_1^*(q_y \eta_1) + C_{22y}\eta_2^*(q_y \eta_2) \\ &+ C_{12y}\eta_1^*(q_y \eta_2) + C_{12y}^*\eta_2^*(q_y \eta_1)]. \end{aligned} \quad (8)$$

We use the same scale units as in Refs. 16 and 17 for length, field and time, except for the order parameters. We here scale η_m by η_0 instead of $\eta_0(T) = \eta_0(1 - T/T_c)^{1/2}$. In our calculations, we typically use the GL parameter $\kappa = 4$, which belongs to a high- κ case, i.e., the order parameter structure is not significantly affected by the internal field distribution.

Calculations are performed in a two-dimensional square area. Outside the open boundary, we set $\eta_1 = \eta_2 = 0$ and $B(\mathbf{r}) = H$ with an applied field H . For the initial state of η_1 , η_2 and \mathbf{A} inside, we use a uniform state at a zero-field. Through the time evolution, vortices penetrate from the boundary. After enough time later, the time-evolution converges and the vortex lattice state is obtained. We analyze this final state.

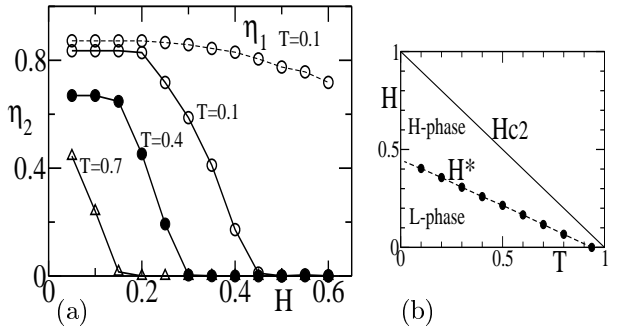


FIG. 1: (a) Maximum of $|\eta_2(r)|$ (solid lines) as a function of $H/H_{c2}(0)$. $T/T_c = 0.1(\circ)$, $0.4(\bullet)$ and $0.7(\triangle)$. η_2 appears at $H < H^*(T)$. For $T/T_c = 0.1$, H -dependence of $|\eta_1|$ is also presented (a dashed line). (b) H - T phase diagram in this GL theory. The transition field H^* and H_{c2} are presented.

We discuss the case when the gradient coupling is absent ($C_{12x} = C_{12y} = 0$). Here, we set $T_{c2}/T_c = 0.95$,

$C_2 = 1$, $C_3 = -C_4 = 0.2$, $c = 0.3$ and $X = 0.5$. In Fig. 1(a), we show the maximum order parameter amplitude at $T/T_c = 0.1$, 0.4 and 0.7 as a function of the external field $H/H_{c2}(0)$ with $H_{c2}(0) = \phi_0/(2\pi\xi_0^2)$. At a critical field $H^*(T)$, the second component η_2 appears as a second order transition. The T -dependence of H^* is shown in Fig. 1(b). This H - T phase diagram qualitatively reproduces the double transition of $\text{PrOs}_4\text{Sb}_{12}$ [4].

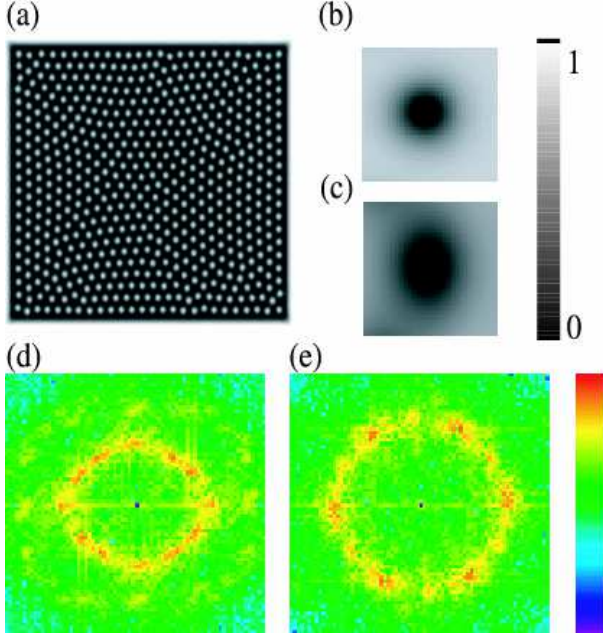


FIG. 2: (a) Density plot of an internal field distribution $B(\mathbf{r})$ at $H/H_{c2}(0)=0.2$ and $T/T_c = 0.1$. White region corresponds to the vortex core with large $B(\mathbf{r})$. Density plot of $|\eta_1(\mathbf{r})|$ (b) and $|\eta_2(\mathbf{r})|$ (c) around a vortex. Diffraction pattern $|B_{\mathbf{q}}|^2$ at $H/H_{c2}(0)=0.2$ [L-phase] (d) and 0.5 [H-phase] (e).

At $H/H_{c2}(0) = 0.2$ and $T/T_c = 0.1$, the vortex distribution is presented in Fig. 2(a), where the internal field distribution is shown as a density plot. There are some domains of the different orientation of the triangular lattice, since the vortex lattice configuration is affected by the boundary. And the triangular lattice is deformed from 60° triangle by the effect of finite c in Eq. (3), coming from the twofold symmetry of $\hat{\phi}_2$. The vortex core shapes of $|\eta_1(\mathbf{r})|$ and $|\eta_2(\mathbf{r})|$ are, respectively, shown in Figs. 2(b) and 2(c). Vortex core shape of $|\eta_2(\mathbf{r})|$ is stretched out toward the y -direction, while that of $|\eta_1(\mathbf{r})|$ remains to be circular. The deformation of the vortex lattice is clear, when we see the form factor of the internal field distribution, as in the neutron scattering experiments. Figure 2(d) shows the “diffraction pattern” $|B_{\mathbf{q}}|^2$ in the L-phase, with the Fourier component $B_{\mathbf{q}} = \sum_{\mathbf{r}} e^{i\mathbf{q}\cdot\mathbf{r}} B(\mathbf{r})$, where we exclude the region near the boundary in the integration over \mathbf{r} . There appear six peaks of the triangular lattice, and the rotated ones for different orientations. These peaks are on an el-

lipse with long axis $2q_x$ and short axis $2q_y$ with the ratio $q_x/q_y \sim 1.2$. For a reference, we also show the diffraction pattern of the 60° triangular lattice in the H-phase in Fig. 2(e), where peaks appear on a circle. The observation of this vortex lattice deformation may be another means to detect the fourfold-twofold transition in the H - T phase diagram.

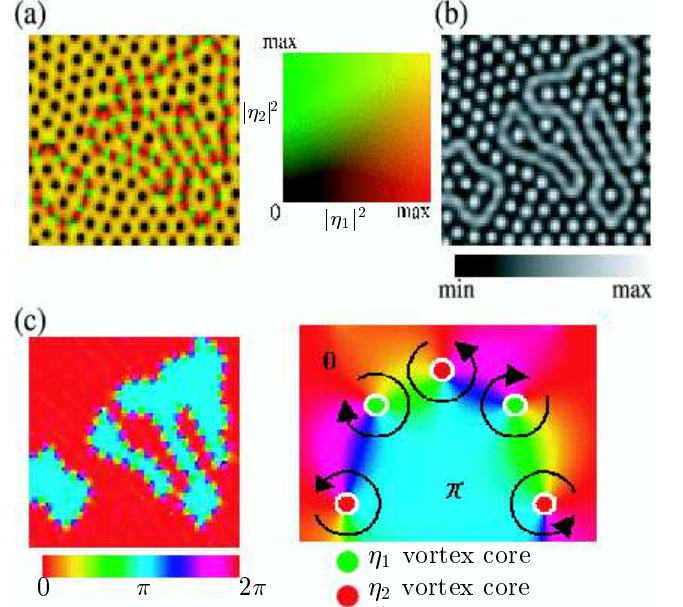


FIG. 3: Vortex structure at $H/H_{c2}(0) = 0.3$ and $T/T_c = 0.1$ [L-phase]. Inside region is focused. (a) Density plot of $|\eta_1(\mathbf{r})|$ and $|\eta_2(\mathbf{r})|$. In the black regions, $|\eta_1|$ and $|\eta_2|$ share a vortex core. Green (red) regions show that only $|\eta_1|$ ($|\eta_2|$) has a vortex core. (b) Internal field distribution $B(\mathbf{r})$. (c) Relative phase $\arg\{\eta_1(\mathbf{r})/\eta_2(\mathbf{r})\}$. Right panel schematically shows relative phase near the vortex sheet appearing at the domain wall.

At higher field in the L-phase, we also find the vortex sheet structure [14] in addition to the regular vortices. We show the spatial distribution of $|\eta_1(\mathbf{r})|$ and $|\eta_2(\mathbf{r})|$ at $H/H_{c2}(0) = 0.3$ in Fig. 3(a). The black circle region presents regular vortex, where $|\eta_1(\mathbf{r})|$ and $|\eta_2(\mathbf{r})|$ share the same vortex core, as seen in Fig. 2(a). The green (red) circle region shows the η_1 - (η_2 -) vortex, where only $|\eta_1(\mathbf{r})|$ ($|\eta_2(\mathbf{r})|$) has vortex core and the other $|\eta_2(\mathbf{r})|$ ($|\eta_1(\mathbf{r})|$) does not. These green and red vortex cores are located alternatively along a loop, forming vortex sheet. In the internal field distribution shown in Fig. 3(b), $B(\mathbf{r})$ has a sharp localized peak at a regular vortex. And large $B(\mathbf{r})$ regions of the vortex core on the vortex sheet are connected each other along the vortex sheet. Each of η_1 - and η_2 -vortices has half flux quantum. If this line structure is found by the direct observation of the internal field distribution, it can be evidence of the vortex sheet appearing in unconventional superconductors. The relative phase of $\eta_1(\mathbf{r})$ and $\eta_2(\mathbf{r})$ are presented in Fig. 3(c). Around the regular vortex, the relative phase is fixed

at $(\alpha + \pi)/2$ or $(\alpha - \pi)/2$ (in our parameter, $\alpha = \pi$). Across the vortex sheet, the relative phase changes from 0 (red region) to π (blue region). This indicates that the vortex sheet appears at the domain wall between the region with the relative phase $(\alpha + \pi)/2$ and that with $(\alpha - \pi)/2$, and that it is not easy to disconnect vortices on the vortex sheet. As shown in the right panel in Fig. 3(c), since windings of the relative phase are opposite at the η_1 -vortex and the η_2 -vortex, the relative phase changes from 0 to π through $\pi/2$ (yellow) or $3\pi/2$ (purple) alternatively between the nearest neighbor vortices along the vortex sheet. Since domains with relative phase $(\alpha \pm \pi)/2$ are degenerate in free energy, we can expect both domains to coexist in sample materials. In the presence of the domain wall between domains, vortex sheet appears when applying field. In our simulation for the penetration process of vortices, boundary region helps creation of the domain wall with vortex sheet structure. The domain wall and vortex sheet are tight structure when coming inside, and survive stably.

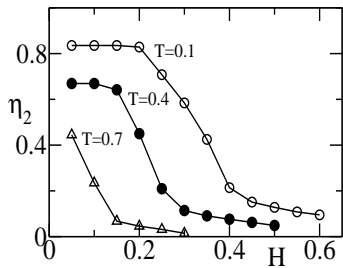


FIG. 4: Maximum of $|\eta_2(\mathbf{r})|$ as a function of $H/H_{c2}(0)$ in the presence of the gradient coupling. $T/T_c = 0.1(\circ)$, $0.4(\bullet)$ and $0.7(\triangle)$. η_2 survives up to $H_{c2}(T)$.

Lastly, we consider the case when the gradient coupling terms do not vanish. We show the results when $C_{12x} = 0.2$ and $C_{12y} = 0$ and the other parameters are kept same. We note that, if we consider the $s+id$ -state (e.g. $\phi_1(\mathbf{k}) \propto 1 - (k_x^4 + k_y^4 + k_z^4)$ and $\phi_2(\mathbf{k}) \propto k_x^4 - k_z^4$) [6], $C_{12y} = 0$. We see the similar vortex structure as in Figs. 2 and 3 in the L-phase. The field dependence of the order parameter maximum of $|\eta_2(\mathbf{r})|$ is shown in Fig. 4. On raising field, $|\eta_2|$ decreases, but it does not vanish at H^* . $|\eta_2|$ has finite value up to $H_{c2}(T)$. Therefore, twofold symmetric order parameter $\eta_2(\mathbf{r})\hat{\phi}_2(\mathbf{k})$ is mixed in addition to the fourfold one $\eta_1(\mathbf{r})\hat{\phi}_1(\mathbf{k})$ in the H-phase [7]. That is, H^* is not a phase transition but the crossover field where η_2 is enhanced in the vortex state. While the anomaly of the second order transition appears at T^* in the zero field case, the anomaly of the phase transition is not observed around H^* at finite fields.

In summary, we investigate the vortex state based on the two-component GL theory in the situation when the fourfold-twofold symmetric superconducting transition occurs. We estimate the transition field H^* where second order parameter η_2 appears. However, H^* is

changed to a crossover field when the gradient coupling terms exist, because the small η_2 survives up to $H_{c2}(T)$. In the L-phase below H^* , the vortex lattice deforms from 60° triangular lattice due to the effect of the twofold symmetric second order parameter. In the two-component superconductor, there is a possibility to observe the exotic vortex structure such as vortex sheet at the domain wall, where two order parameters have different vortex cores and these cores are alternatively located along a line. These characters of the vortex structure may be clear evidence of the fourfold-twofold symmetric double transition and unconventional multi-component superconductivity, if they are experimentally observed.

We would like to thank K. Izawa, Y. Matsuda, Y. Aoki, N. Nakai and M. Takigawa for fruitful discussions.

* Electronic address: matsunaga@mp.okayama-u.ac.jp
 † Electronic address: oka@mp.okayama-u.ac.jp
 ‡ Electronic address: machida@mp.okayama-u.ac.jp

- [1] E.D. Bauer, N.A. Frederick, P.-C. Ho, V.S. Zapf, and M.B. Maple, Phys. Rev. B **65**, 100506 (2002).
- [2] H. Kotegawa, M. Yogi, Y. Imamura, Y. Kawasaki, G.-q. Zheng, Y. Kitaoka, S. Ohsaki, H. Sugawara, Y. Aoki, and H. Sato, Phys. Rev. Lett. **90**, 027001 (2003).
- [3] R. Vollmer, A. Faißt, C. Pfleiderer, H.v. Löhneysen, E.D. Bauer, P.-C. Ho, V. Zapf, and M.B. Maple, Phys. Rev. Lett. **90**, 057001 (2003).
- [4] K. Izawa, Y. Nakajima, J. Goryo, Y. Matsuda, S. Osaki, H. Sugawara, H. Sato, P. Thalmeier, and K. Maki, Phys. Rev. Lett. **90**, 117001 (2003).
- [5] Y. Aoki, A. Tsuchiya, T. Kanayama, S.R. Saha, H. Sugawara, H. Sato, W. Higemoto, A. Koda, K. Ohishi, K. Nishiyama, and R. Kadono, Phys. Rev. Lett. **91**, 067003 (2003).
- [6] J. Goryo, Phys. Rev. B **67**, 184511 (2003).
- [7] M. Ichioka, N. Nakai, and K. Machida, J. Phys. Soc. Jpn. **72**, 1322 (2003).
- [8] T.A. Tokuyasu, D.W. Hess, and J.A. Sauls, Phys. Rev. B **41**, 8891 (1990).
- [9] K. Machida, T. Fujita, and T. Ohmi, J. Phys. Soc. Jpn. **62**, 680 (1993).
- [10] T. Fujita, W. Aoyama, K. Machida, and T. Ohmi, J. Phys. Soc. Jpn. **63**, 247 (1994).
- [11] Y. Hirano, F. Fujita, K. Machida, and T. Ohmi, J. Phys. Soc. Jpn. **64**, 210 (1995).
- [12] T. Kita, Phys. Rev. Lett. **83**, 1846 (1999).
- [13] M.M. Salomaa and G.E. Volovik, Rev. Mod. Phys. **59**, 533 (1987).
- [14] Ü. Parts, E.V. Thuneberg, G.E. Volovik, J.H. Koivuniemi, V.M.H. Ruutu, M. Heinilä, J.M. Karimäki, and M. Krusius, Phys. Rev. Lett. **72**, 3839 (1994).
- [15] For example, N. Schopohl and L. Tewordt, J. Low Temp. Phys. **41**, 305 (1980).
- [16] R. Kato, Y. Enomoto, and S. Maekawa, Phys. Rev. B **47**, 8016 (1993).
- [17] M. Machida and H. Kaburaki, Phys. Rev. Lett. **71**, 3206 (1993).